Chapter 5

Electrochemical Reactivity at Free and Supported Gold Nanocatalysts Surface

Seydou Hebié, Yaovi Holade, Karine Servat,
Boniface K. Kokoh and Têko W. Napporn

Additional information is available at the end of the chapter

http://dx.doi.org/10.5772/64770

Abstract

This chapter presents an overview on size, structure, morphology, composition as well as the effect of the support on the electrocatalytic properties of gold nanoparticles (AuNPs). It was found that the electrocatalytic properties of unsupported AuNPs strongly depend on their size and shape. Consequently, the electrocatalytic properties of AuNPs can be tuned. Furthermore, to design high-performance electrocatalysts with minimal precious metal content and cost, the direct immobilization of metal NPs onto carbon-based substrates during their synthesis constitutes another elegant alternative and has been thoroughly examined. These "easy-to-use" supports as scaffolds for AuNPs, namely carbon black, carbon paper, etc., offer beneficial contributions. Indeed, thanks to their high available surface area, good electronic conductivity and synergistic effect between the chemical species present on their surface and the loaded NPs, carbon-based supports enable maximizing the efficient utilization of the catalysts toward drastic enhancement in both activity and durability. We also examined different judicious combinations of (electro)analytical techniques for the unambiguous determination of the reaction product(s) over the Au-based nanocatalysts, using glucose as model molecule given its importance in electrocatalysis. The performances of carbon-supported AuNPs as anode materials in direct glucose fuel cell in alkaline medium were also discussed.

Keywords: gold nanoparticles, electrocatalysis, oxidation, glucose, fuel cells

1. Introduction

During several decades, bulk gold has been considered as less active material, but at nanoscale, it exhibits surprisingly physicochemical and catalytic properties. Such properties depend on the size, the morphology, and the surface structure of the nanoparticles. Different synthesis approaches have paved the way of controlling the size, shape, and crystallographic structures of gold nanoparticles (AuNPs) in order to tune their (electro)catalytic activity. The control of these key parameters enables designing highly effective and durable gold catalysts for potential applications not only in sensors, electrochemical reactors, and fuel cells but also over electrochemical field. In electrocatalysis, the surface structure of the electrode material plays a key role. Thereby, the preparation of active and efficient nanomaterials becomes a challenge to be taken up. It is known that various gold nanomaterials exhibit relevant ability toward the oxidation of organic molecules. Therefore, the electrocatalytic activity of different AuNPs toward the glucose oxidation in alkaline electrolyte was described in the literature [1–5]. On AuNPs, this reaction is size, shape, and structure dependent. The goal of this chapter was to address the recent advances in the preparation of free and carbon supported AuNPs and their performance in electrocatalysis. Precisely, factors affecting the growth mechanism and the synthesis processes are presented. Furthermore, discussion on the electroactivity of synthesized AuNPs toward biomass-based compounds (glucose…) and their performances in fuel cells and/or the production of sustainable added-value chemicals from selective oxidation will be extensively reported.

2. Electrochemical reactivity at free and supported gold nanocatalysts surface

2.1. Growth of gold nanoparticles in solution

The preparation of metal nanoparticles in solution involves systematically two important processes, which are the nucleation followed by the growth of the nanoparticles.

2.1.1. Theoretical aspects: nucleation and reaction-limited growth

Key concepts that enable the understanding of reactions limiting the nucleation and the growth processes need to be reminded. On the kinetic point of view, it is recognized that the nucleation step is very fast and cannot be observed by a usual transmission electron microscope. In a typical metallic nanoparticles synthesis, the precursor compound containing the metal cation is reduced or decomposed to metallic atoms (zero oxidation state) that will coalesce to form nanoparticles. La Mer and Dinegar proposed a mechanism for explaining the nucleation process as follows [6] (**Figure 1**).

http://dx.doi.org/10.5772/64770

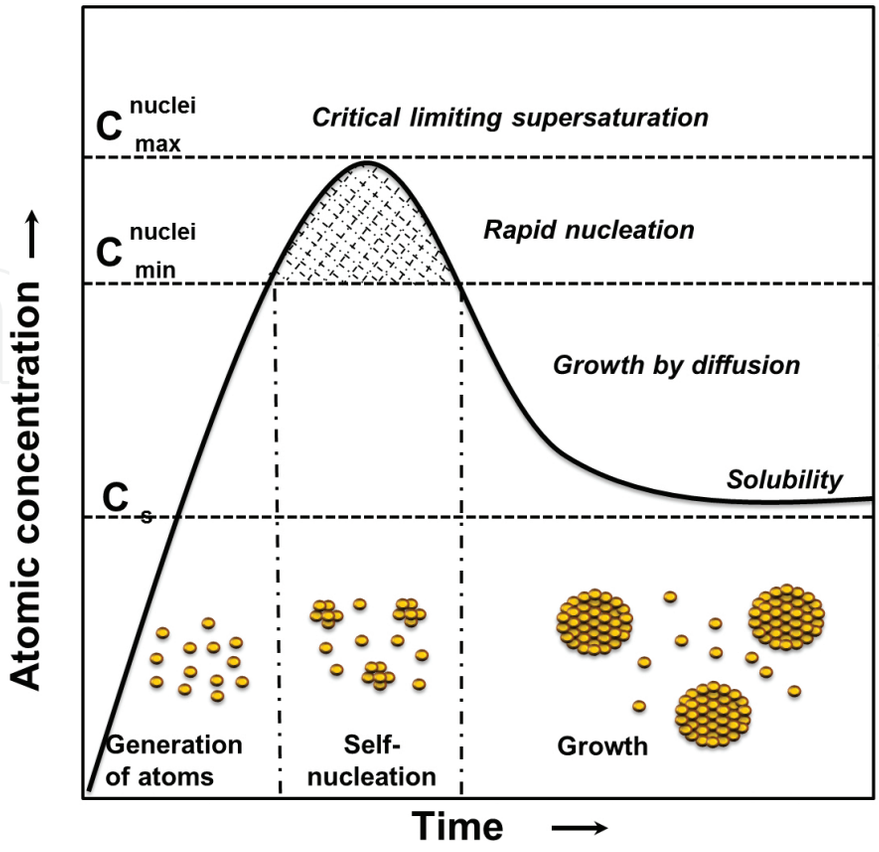

Figure 1. Schematic illustration of La Mer's nucleation condition. Reprinted and adapted with permission from [6]. Copyright © 1950, American Chemical Society.

According to this mechanism, the concentration of metal atoms increases rapidly during the nucleation, as regularly as the precursor is reduced. The reduction reaction can be promoted by ultrasonication or by raising the temperature. Once the concentration of nuclei reaches a critical point so-called point of supersaturation, they start aggregating into small clusters *via* a self-nucleation process in the case of homogeneous nucleation. Then, the nuclei grow rapidly by consuming the metal atoms present in the bulk solution. Thereby, a decrease in the concentration of the single atoms in the solution is observed. If the monomer concentration falls rapidly below the supersaturation, the nucleation ends, and only the nuclei already present in the reaction mixture will grow to nanoparticles with homogeneous size distribution. With the continuous supply of the atoms due to the reduction in the metal precursor, the nuclei grow to larger nanoparticles until the establishment of an equilibrium state between the atoms at the surface of the nanoparticles and those in the solution. Once the clusters reach a critical size, structural changes require significant energy input so that the clusters grow in a well-defined structure leading to the formation of seeds. The key strategy in synthesizing nanoparticles with controlled-shape is to ensure meticulous monitoring of the seeds population with different internal structures. Thermodynamic and kinetic factors are important for controlling the nucleation process. The heterogeneity of nanostructured seeds is determined by the surface free energies of the different species in combination with the kinetic effects on the generation and the addition of metal atoms to the nuclei. Different theories have been

developed for understanding the mechanism of nanoparticle growth process [7, 8]. Due to the small size of the clusters, they have high surface-to-volume ratio. As a result, very small particles exhibit a significant surface excess energy, which is a non-negligible percentage of the total energy. Therefore, the formation of larger particles results from a solution, which is not initially at thermodynamic equilibrium and leads to a decrease in the surface energy. Thereby, it plays a crucial role in the growth of nanocrystals. A colloidal particle grows by a sequence of monomer diffusion toward the surface followed by the reaction of the monomers at the surface of the nanocrystal. The classical theory by Lifshitz and Slyozov [9] and Wagner [10] (referred as LSW) has dominated researchers thinking about precipitate coarsening. In fact, the LSW theory driven by the reduction in the surface energy was proposed by Ostwald in 1901 [11]. A key idea of this theory is that coarsening or Ostwald ripening results from the interaction of particles embedded within a matrix phase. Coarsening effects, controlled by the mass transport (most frequently the diffusion), are often termed the Ostwald ripening process. The diffusion process is dominated by the surface energy of the nanoparticle. The interfacial energy is the energy associated with an interface due to the difference between the chemical potential of atoms in an interfacial region and atoms in neighboring bulk phases. The LSW theory, considering a diffusion-limited growth, was able to make quantitative predictions on the long-time behavior of the coarsening process. The LSW approach examines the growth of spherical particles in a supersaturated medium and is based on basic assumptions extensively described in the literature [7–10].

2.1.2. Free and supported gold nanoparticles for electrocatalysis

2.1.2.1. Size and shape-controlled gold nanoparticles

The electrochemical properties of metal NPs are strongly influenced by their size, shape, and structure. This dependence has motivated the development of a variety of synthesis methods for controlling their size and shape. Thus, the synthesis of most gold nanoparticles (AuNPs) is established, in terms of degree of control over the size, shape, monodispersion, and in the understanding of the growth mechanism.

- *Spherical gold nanoparticles*

In the early 1951, the most popular Turkevich synthesis method, later refined in the 1970s by G. Frens [12], was developed to yield quasi-spherical and mono-dispersed AuNPs in water through a small amount of hydrochloroauric acid as a precursor and sodium citrate solution [13]. The mean size of the particles ranged from 5 to 200 nm. The mixture was heated to boiling. In this synthesis, the citrate ions adsorb on the surface of the nanoparticles by creating a negatively charged layer. This stabilizes and prevents the nanoparticles from aggregation by providing a sufficient electrostatic repulsion between the particles. In the early 1990s, Brust et al. [14] have developed a method to synthesize AuNPs in organic medium based on the reaction of hydrochloroauric acid, the tetraoctylammonium bromide (TOAB), and the sodium borohydride in toluene [14]. The gold nanoparticles were small from 2 to 6 nm. $NaBH_4$ was the reducing agent, while TOAB played both the role of intermediary transfer phase and

http://dx.doi.org/10.5772/64770

surfactant. After 24 h of stirring, two phases were separated. The organic phase was successively washed with dilute sulfuric acid and distilled water. These clusters have attracted much attention due to their small size. However, due to the toxicity of organic solvents as toluene and the surfactant or molecule-like properties (high affinity with catalytic actives sites), electrocatalytic applications are somewhat limited. To overcome this passivation effect due to the strong adsorption of surfactant at AuNPs surface, we have recently revisited the synthesis method initially developed by Slot and Geuze to yield spherical AuNPs [15]. Based on an empirical Taguchi model, Habrioux et al. [16] adapted this synthetic method to find experimental conditions and optimal synthesis parameters to yield spherical AuNPs, monodisperse in size ranging from 3 to 17 nm. In this synthesis, two solutions are separately prepared: one containing the gold salt solution and the second is a mixture of tannic acid and sodium citrate as reported [15, 16]. Then, AuNSs-10 and AuNSs-4 samples (the number after ANSs represents the mean particles size) were obtained. Here, due to its long carbon chain, tannic acid acts as a surfactant for the control of gold particles shape and size, while a trisodium citrate solution serves as reducing agent. Slot and Geuze [15] indicated that the concentration of tannic acid in the reducing solution, the temperature and pH of the solution are important parameters in the size control. When the pH is adjusted between 7.5 and 8 by adding a few drops of 0.1 mol L^{-1} NaOH solution and the temperature is set at 60°C, monodispersed nanoparticles can be obtained by varying the amount of tannic acid [15].

In addition, spherical AuNPs can also be synthesized by the reduction in gold salts by sodium borohydride in the presence of CTAB as surfactant [3–5]. After the appropriated time and amount of chemicals as reported, AuNPs with different sizes can be obtained in particular AuNSs-6 and AuNSs-14 samples, respectively. It is important to notice that CTAB has strong interaction with AuNPs surface. However, we have shown that it is possible to remove it electrochemically.

Figure 2 shows the TEM and HRTEM images and the corresponding particles size distribution of different synthesized spherical NPs. The AuNPs are homogeneous in size and shape. However, the AuNSs-14 sample is polydispersed in size due to the overgrowth effect of gold particles during the ageing time of this sample [17]. Characteristically, the average particle sizes are 4.2 ± 0.7, 6.2 ± 1.2, 10.3 ± 1.4, and 14.7 ± 2.9 nm for AuNSs-4, AuNSs-6, AuNSs-10, and AuNSs-14, respectively, from the gold solution during the synthesis; AuNSs-10 and AuNSs-4 are spherical AuNPs obtained from the Slot synthesis method with 8 and 12 mL of tannic acid, respectively.

As can be seen in **Figure 2(A–D)**, the HRTEM images of all AuNSs samples present mostly (1 1 1) facets. In fact, one can consider that the nanoparticles obtained by the Slot method are mainly decahedron delimited by (1 1 1) facets. The kinetic growth in the {100} direction seems to be superior to that in the {1 1 1} direction, which promotes the development of (1 1 1) facets. The measured interplanar spaces for all lattice fringes from high-resolution transmission electron microscopy images correspond to the values obtained from electron diffraction and XRD data [18, 19]. As an example, the measured interplanar space of 2.35 Å is in good agreement with the (1 1 1) lattice plane of face-centered-cubic (fcc) of gold [18, 19]. The surface energy (γ) associated with different crystallographic facets of fcc metal types is described as

follows: $\gamma(1\,1\,1) < \gamma(1\,0\,0) < \gamma(1\,1\,0)$ [20]. This order fully justified from a thermodynamic point of view the preferential formation of (1 1 1) facets on the surface of seeds. In addition, the (1 0 0) facet is also observed in the AuNSs-14 sample.

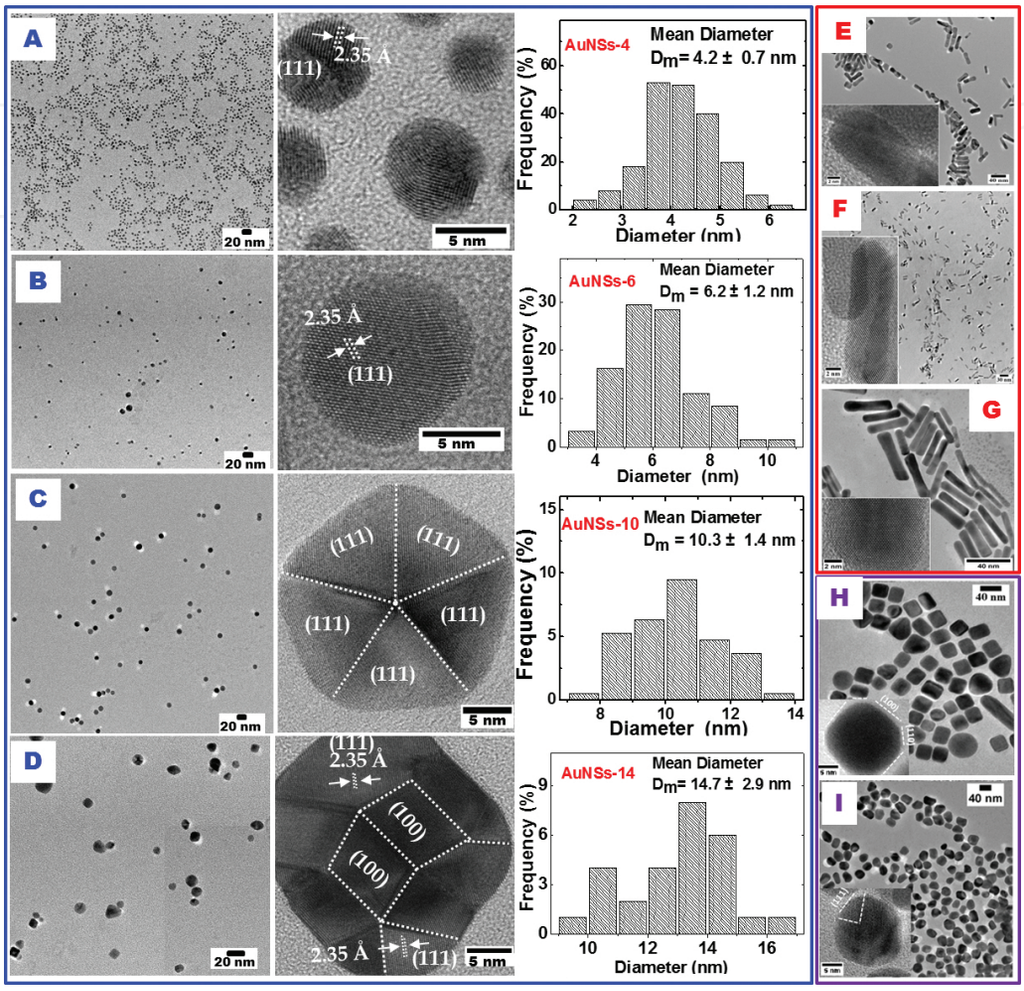

Figure 2. Typical TEM, HRTEM micrographs, and corresponding size distribution of spherical AuNPs (A) AuNSs-4, (B) AuNSs-6, (C) AuNSs-10, and (D) AuNSs-14, (E) AuNRs-E, (F) AuNRs-F, (G) AuNRs-G, (H) AuNCs, and (I) AuNPoly materials. (A–D) Reprinted and adapted with permission from Ref. [3]; Copyright 2016, John Wiley & Sons, Inc. (E–G) Reprinted and adapted with permission from Ref. [5]; Copyright © 2013, American Chemical Society. (H–I) Reprinted and adapted with permission from Ref. [4]; Copyright © 2013, The Author(s).

• *Anisotropic gold nanoparticles*

Different approaches have been developed to yield anisotropic AuNPs by the wet chemical method. Among them, the seed-mediated growth was employed to synthesize a wide range of size and shape controlled nanoparticles [21–23]. The process is generally carried out in two steps: nucleation followed by the growth step. Both steps may be performed in the same or separate reactors. In the growth stage of NPs, the reaction conditions for the shape-controlled are less severe than those for the seeds preparation. The activation energy for the reduction in the metal precursor on a particle already formed is much lower than that required for

http://dx.doi.org/10.5772/64770

homogeneous nucleation of seeds in the same solution [24]. Therefore, the control of the morphology can be considered as the process of proliferation of seeds. The growth of particles is progressively done by the reduction in the metal precursor to the surface of seeds. The metal atoms formed are deposited onto the surface of the seeds, then diffuse to reach a site where they will find atoms of low coordination leading to an increase in the particle size. This dynamic interaction of growth and dissolution conducts the evolution of seeds in nanocrystals. The general strategy in controlling the shape in the growth of nanoparticles is to stabilize a particular facet through a molecular interaction by using a surfactant. Chemisorption of a surfactant has a strong influence on the final shape and structure of the nanoparticle. Actually, it plays an important role in the growth kinetics of the facets since its adsorption at the surface of the seeds reduces the surface free energy and promotes the stabilization of the nanocrystal. Interestingly, surfactant has a preferential affinity with a particular surface orientation, which can promote interactions between atoms during the growth process [25]. During a synthesis for example, if the seeds are truncated octahedrons with crystallographic planes (1 1 1) and (1 0 0), the selective adsorption of a surfactant on the planes (1 0 0) will cause the decrease in the rate of growth of these facets and block their access.

• *Case of gold nanorods*

A very large number of articles cover the synthesis of gold nanorods (AuNRs) by the seed-mediated growth [26–28]. The original idea was that surfactants such as cationic micelles could serve as a template mode to guide the growth and provide colloidal stability [23]. However, the role of the seeds is also critical. The aspect ratio can be precisely controlled by varying the amount of seed in the growth solution [26]. Furthermore, the presence of small amounts of silver nitrate in the synthesis has a dramatic effect on yield, and the final shape of the particle [29]. Many hypotheses have been advanced to explain the mechanism by which the Ag(I) ions react and alter the kinetics of growth, structure, and the formation of the AuNRs. A significant contribution for understanding the roles of the ions Ag(I) and the crystal structure of the seed was provided by Liu and Guyot-Sionnest [30]. They found that the AuNRs synthesis yield increases by regulating the pH value of the reaction between 2 and 4 and by increasing the reaction time from 1 to 2 h. Additionally, it was issued by Jana et al. [23], in the presence of CTAB, that the bromide anion and Ag(I) precipitate to form AgBr which will adsorb at the seeds surface during the growth process. When AgBr is adsorbed, the crystal facets are blocked, and therefore, their growth is restricted. Under acidic pH conditions, the adsorption of Ag(I) is favored and outweighs the reduction in silver atom [31]. Thereby, the aspect ratio of AuNRs can be controlled by adjusting the amount of Ag(I) in the growth solution [29, 32]. Sau and Murphy [33] showed the influence of the amount of seeds on the aspect ratio and the diameter of AuNRs. Following these observations, Nikoobakht and El-Sayed [29] have proposed that CTAB forms a flexible template whose size is dependent on its concentration and ionic strength of the solution. Thus, the Ag(I) ion and the polar heads of CTAB may be considered as pairs of AgBr. In this way, the charge density of the bromide ions decreases. Therefore, repulsion between adjacent polar heads on the gold surface leads to the template elongation of CTAB [29]. Wang [34] showed that CTAB monomers had a higher affinity for the lateral facets which were particularly favored, compared to the facets at the ends due to the van der Waals

interactions between the nonpolar channels tail of CTAB. Unlike the previous mechanism, Murphy's group [33, 35] proposed a mechanism whereby a rigid structure of CTAB monomers helps to maintain a unidirectional growth by "zipping" mechanism. The presence of Ag(I) ions enables controlling the reduction kinetics of gold salt. Indeed, the adsorption of AgBr on the surfaces of gold nanocrystals promotes the development of high-energy sides composed of (1 1 0) facets and allows the growth of monocrystalline rods [30]. According to Liu and Guyot-Sionnest [30], in the synthesis conditions (acidic media), a silver monolayer can be deposited onto the lateral (1 1 0) facets driven poisoning of these surfaces. The growth kinetics of these facets is then slowed down, and the anisotropic growth might not be made from silver facets. This mechanism is the basis of unidimensional growth of monocrystalline nanocylinder.

Based on the synthesis procedure developed by Murphy's group [33], AuNRs were prepared at a constant temperature of 27°C by a modified seed-mediated growth method. The seed solution was prepared as described in the literature [5]. The AuNRs obtained have an aspect ratio of 3.3 ± 0.7 for an average length of 33.2 ± 6.0 nm. The AuNRs solution is called AuNRs-E (**Figure 2E**).

Based on the seed mediated growth, we have synthesized AuNRs by mixing growth solution and $NaBH_4$ in the same reactor [5]. This permits to produce *in situ* the seeds followed by the growth of the AuNRs. The obtained AuNRs were named AuNRs-F. The AuNRs-F have an aspect ratio of 2.54 ± 0.68 for an average length of 14.18 ± 2.93 nm (**Figure 2F**).

The AuNRs can be also synthesized by one-step method without any use of seeds solution. In fact, the seeds are generated *in situ* in the same solution. This method, developed by Tollan et al. [36], is based on the particular reducing and stabilizing properties of acetylacetone (acac) and stabilizing properties of CTAB. Thus, in the presence of CTAB, silver ions and at moderate pH, acac reduces the gold precursor and promotes the growth of nanorods. It is well known that acac is a good organic diketone chelate ligand [37]. In the presence of gold salt $HAuCl_4$, it can complex to form a stable chelate Au(III)-acac which can decompose under ambient conditions to form spherical nanoparticles of variable size (10–40 nm). The kinetics of the reduction depends on the pH value. It is slower in high pH due to the ease of ligands transformation into enoles. Under these conditions, the chelates are stable and a smaller particles size is obtained. In the case of the AuNRs synthesis, chelates Au(III)-acac in a basic medium that provides enolates may reduce the gold salt. When the pH value is higher than 10, the nucleation is rapid, thereby the formed nuclei will aggregate fast, leading to the formation of spherical particles. It seems that the seeds generated *in situ* keeps getting bigger under the same conditions as those of the seed-mediated growth process in the presence of CTAB and Ag(I) in AuNRs [36]. The fabricated AuNRs were named AuNRs-G. The AuNRs-G has an aspect ratio of 4.90 ± 1.06 for an average length of 34.27 ± 7.28 nm (**Figure 2G**).

Gold nanocuboids (AuNCs) can be synthesized by seed-mediated growth process in the presence of copper ions. This method is based on the same procedure as for AuNRs-E preparation, but the Ag(I) cation is replaced by the Cu(II) one. Sun et al. [19] showed that the formation of AuNCs is related to both preferential (1 1 1) facets poisoning by the cations Cu(II) and CTAB. Indeed, the presence of these two species affects significantly the surface energy of the different facets of the crystal due to their preferential adsorption and therefore the

http://dx.doi.org/10.5772/64770

growth kinetics of the different facets of the crystal. As described in the literature, the seeds produced in the presence of CTAB have (1 1 1) facets more accessible to the solvent as the (1 0 0) facets appear to have a greater affinity with the CTAB than the (1 1 1) facets [38]. When introduced into the growth solution, the Cu(II) cations are adsorbed preferentially on the readily accessible (1 1 1) facets and decrease the kinetics of growth in this direction in accordance with their concentration. Therefore, nanocuboids and nanodecahedrons are obtained based on the amount of Cu(II) ions. These authors showed that when the concentration of Cu(II) was 0.2 mmol L^{-1}, the copper ions were selectively adsorbed on the (1 1 1) facets and the kinetics of growth in the (1 1 1) direction is reduced but still remained higher than that in the (1 0 0) direction, which led to AuNCs. However, when the concentration of Cu(II) ions increases up to 1.6 mmol L^{-1}, the growth kinetics of the (1 1 1) direction is much slower. The average particle size is 29 ± 3 nm with mostly (1 0 0) facets at the edges and (1 1 1) facets at the corners (**Figure 2H**).

With a procedure similar to that described above, we were able to obtain polyhedrons. Typically, 12.5 μL of 1.0×10^{-2} mol L^{-1} silver nitrate and 12.5 μL of 1.0×10^{-2} mol L^{-1} $CuSO_4$ were jointly added. Finally, 1.25 μL of the seed solution was added to the growth solution at 25°C. The combination of silver and copper ions promotes the polyhedrons formation with 37 nm in size. The average particle size is 36.8 ± 4.9 nm with mostly (1 1 1) facets (**Figure 2I**).

2.1.2.2. Synthesis of gold nanoparticles supported on carbon substrates

Carbon-supported AuNPs can be synthesized from various bottom-up approaches, including the polyol [39], water-in-oil (w/o) microemulsion [40, 41]. The w/o method has been initiated by Boutonnet et al. [41] in 1982 when they reported the successful preparation of Pt, Pd, Rh, and Ir NPs with sizes of 3–5 nm. Then, it has been successfully used to prepare various metallic nanomaterials such as Au [40] for electrocatalytic tasks. Unfortunately, the nature of the surfactants (Brij®30, PVP, etc.) and their strong adsorption at the NPs surface constitutes the main drawback of the w/o and other surfactant-based methods. As the majority of the methods for synthesizing noble metal NPs involve surfactants, which are undesired for electrocatalysis application because of their adsorption on catalytic sites, elegant methods for the direct "printing" of AuNPs onto carbon papers or fibers to be used directly in electrocatalysis have been initiated. **Figure 3A** shows the SEM image of AuNPs embedded in electrospun carbon fibers (CFs) at the metal loading of 26 wt.% [42]. In typical experiment, $HAuCl_4$ is first mixed into preheated N,N-dimethylformamide (DMF) at 70°C, followed by the slow addition of polyacrylonitrile (PAN, M_W = 150,000) and stirred for 3 h. The obtained electrospun felts are stabilized in air at 250°C for 2 h and then carbonized at 1000°C for 1 h under N_2. The resulting sample is composed of pure CFs ~240 nm diameter and Au@CFs ~700 nm. As displayed in **Figure 3A**, the gold particle size is heterogeneous from 50 to 250 nm. In addition, it was found that 12.2 wt.% of Au particles are located inside the fibers, thus inaccessible. Furthermore, the group of Hsin-Tien Chiu has developed several electrodeposition methods that enable the growth of Au nanostructures on carbon paper: nanoparticles (**Figure 3B**), nanocorals (**Figure 3C**), and branched belt (**Figure 3D**) [43, 44]. The electrodeposition is achieved by applying a voltage of 1.6–1.8 V for at least 18 h in an aqueous mixture of $HAuCl_4$,

$NaNO_3$, and cetyltrimethylammonium chloride (CTAC). The surfactant CTAC acts as a capping agent to reduce the surface energy and controls the growth and shape of nanostructures, while NO_3^- is expected to increase the conductivity of the solution and oxidize less stable Au facets back into $AuCl_4^-$ [44, 45]. This leads to a high Au amount (>2.5 mg cm^{-2}) [44]. The electrochemical characterizations combined TEM (**Figure 3E**) and selected area electron diffraction (SAED) pattern (**Figure 3F**) suggested that the surface structure of the nanocorals resembles that of the branched belt, with highly exposed Au(1 1 0) planes [43]. The presence of exposed Au(1 1 0) surfaces is known to promote the glucose oxidation [2]. Overall, these methods allow passing through the intermediate carbon black that leads to NPs detachment during the reaction. However, it should be noticed that the particles size is relatively high and the remaining CTAC might limit the accessibility to some active sites.

Notwithstanding these successful demonstrations, carbon paper-based methods remain questionable since they give high loading of precious metals and larger particles size, which substantially decrease the effectiveness of the catalyst. On the other side, the retained molecules at the surface of NPs from chemical methods decrease notably the catalytic performances of the obtained electrodes due to the inaccessibility of some active sites that are obviously blocked. Therefore, the exploration of other alternatives to minimize the use of organic molecules that have an affinity with the NPs surface and decrease the noble metal content in the catalyst is desired. The so-called *bromide anion exchange* (BAE) method, a bottom-up approach, has been initiated since 2012 to meet these requirements by fabricating advanced surfactant-free metal NPs for electrochemical energy conversion technologies [46–48]. The main feature of this method lies in its simplicity of implementation by using only potassium bromide (KBr) as surfactant/capping agent. Halide ions (Cl^-, Br^-, I^-) may serve as coordination ligands and thus play the role of capping agent for shape and size control of NPs [49]. In a standard procedure of BAE, Au precursor salt is dissolved in water at 25°C followed by the addition of KBr. Afterwards, a given amount of carbon black is added under ultrasonic homogenization for 45 min, followed by the dropwise addition of the reducing agent. Thereafter, the temperature is raised at 40°C for 2 h. Finally, metal NPs supported on carbon black are filtered, washed with ultra pure water, and dried in an oven at 40°C for 12 h. Before the reduction step, the change of the solution color (from a clear yellow to a deep yellow) can be observed upon the addition of KBr [48]. This change supported by UV-vis measurements [50] is assigned to the ligand-to-metal charge transfer transition phenomenon in metal complex ions because of the partial substitution of Cl^- by Br^-, yielding to $[AuCl_{4-x}Br_x]^-$, $0 \leq x \leq 4$. Br^- being bigger than Cl^-, a mixed complex ion $[AuCl_{4-x}Br_x]^-$ is expected to provide more steric environment than $[AuCl_4]^-$. Hence, it could better control the particles size/shape growth after the reduction. **Figure 4A** shows the TEM image of Au/C and highlights well-dispersed 3–10 nm AuNPs. The HRTEM image shows an octahedron shape having different degrees, with crystallographic (1 1 1) and (2 0 0) facets. For supported NPs, the formation of facets (1 1 1) and (1 0 0) is thermodynamically more favorable since the surface energy (γ) associated with different crystallographic planes is $\gamma(1\ 1\ 1) < \gamma(1\ 0\ 0) < \gamma(1\ 1\ 0)$. Thus, the polyhedron corresponding to the more stable thermodynamic morphology (Wulff's theorem) for a nanoparticle with face-centered cubic crystal symmetry is a truncated octahedron. Furthermore, the presence of the carbon support undoubtedly influences the final shape. Obtaining high Miller

http://dx.doi.org/10.5772/64770

indices such as (2 0 0) instead of (1 0 0) suggests that the BAE synthesis method offer favorable thermodynamic conditions. **Figure 4B** displays the high-resolution X-ray photoelectron spectroscopy (XPS) spectrum of the Au 4f core level. The observed doublets are related to spin-orbit splitting (3 ± 1/2) with binding energies of 83.9 (Au $4f_{7/2}$) and 87.6 eV (Au $4f_{5/2}$). The presence of AuO_x is indicated by doublets at 85.5 (Au $4f_{7/2}$) and 89.1 eV (Au $4f_{5/2}$). Energy-dispersive X-ray (EDX) spectroscopy and X-ray diffraction (XRD) have regardless shown that the oxide amount is negligible [51]. Indeed, upon exposure to ambient air, a thin protective layer safeguards the metal surface from deep oxidation. The total metal loading determined from the thermogravimetric analysis was 21 wt.% on the basis of 20 wt.% and Au/C was produced with a high synthesis yield greater than 94% [51].

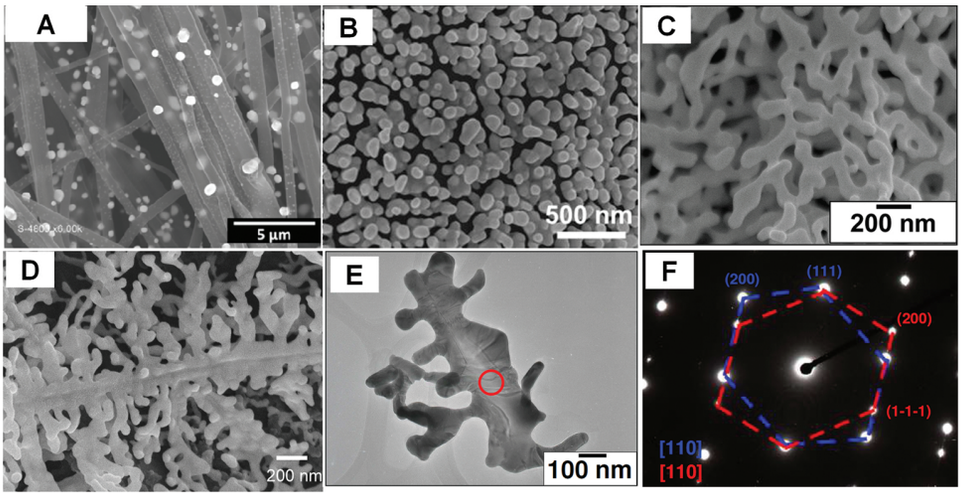

Figure 3. (A) SEM image of AuNPs embedded in electrospun CFs. SEM images of the electrochemically growth Au nanostructures on carbon paper: (B) nanoparticles, (C) nanocorals, (D) branched belt. (E) TEM micrograph of a branched belt and its corresponding SAED pattern (E): red circle region shown in (F) and highlighting the superposition of two sets of diffraction patterns (blue and the red dotted lines) with [110] zone axis. (A) Reprinted and adapted with permission from Ref. [42]; Copyright 2016, John Wiley & Sons, Inc. (B) Reprinted and adapted with permission from Ref. [44]; Copyright 2012, RSC. (C–F) Reprinted and adapted with permission from Ref. [43]; Copyright 2014, ACS.

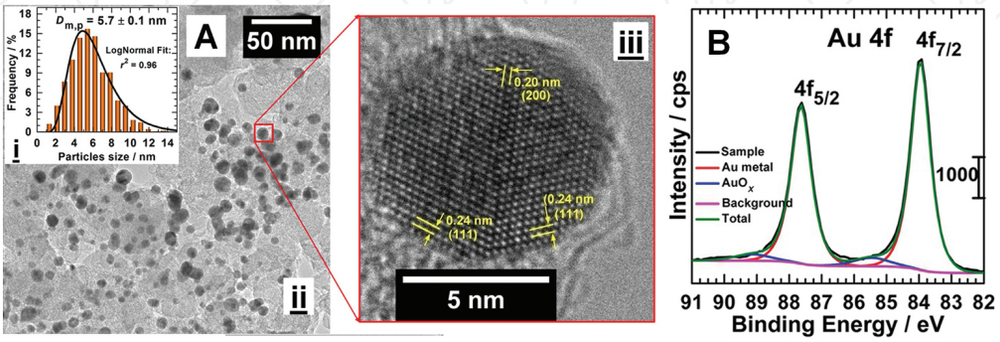

Figure 4. AuNPs dispersed on Vulcan XC 72R carbon (20 wt% Au/C, from BAE method). (A) TEM image and (i) inset the histogram of the nanoparticles size distribution: (ii) overview and (iii) close view that shows HRTEM micrograph of one nanoparticle ([101] zone axis). (B) High-resolution XPS spectra of the Au 4f core level. Reprinted and adapted with permission from Ref. [51]; Copyright 2016, John Wiley & Sons, Inc.

3. Electrochemical characterization of gold nanoparticles surface in aqueous media

3.1. Cyclic voltammetry in alkaline solution

Among the surface chemistry techniques, cyclic voltammetry is particularly an efficient, size, and structure sensitive tool in electrochemistry for analyzing and probing the electrode material surface. **Figure 5** displays the typical cyclic voltammograms of the different synthesized AuNPs electrodes in 0.1 mol L^{-1} NaOH recorded at 20 mV s^{-1} and 20°C. As can be seen, each CV shows three main regions: a large double layer region followed by the adsorption of hydroxyl OH^- species from 0.6 V vs. RHE. Afterwards, the oxidation and reduction regions of gold oxides can be observed.

During the positive scan, the large capacitive current associated with the double layer region is typical electrochemical behavior of gold material. This behavior of the gold electrode in the double layer region as well as the surface oxidation region is structure dependent as evidenced by Kokoh et al. [3, 4] on size and shape controlled gold nanoparticles and Hamelin [52] on gold single-crystal Au (1 1 1) and Au (1 0 0).

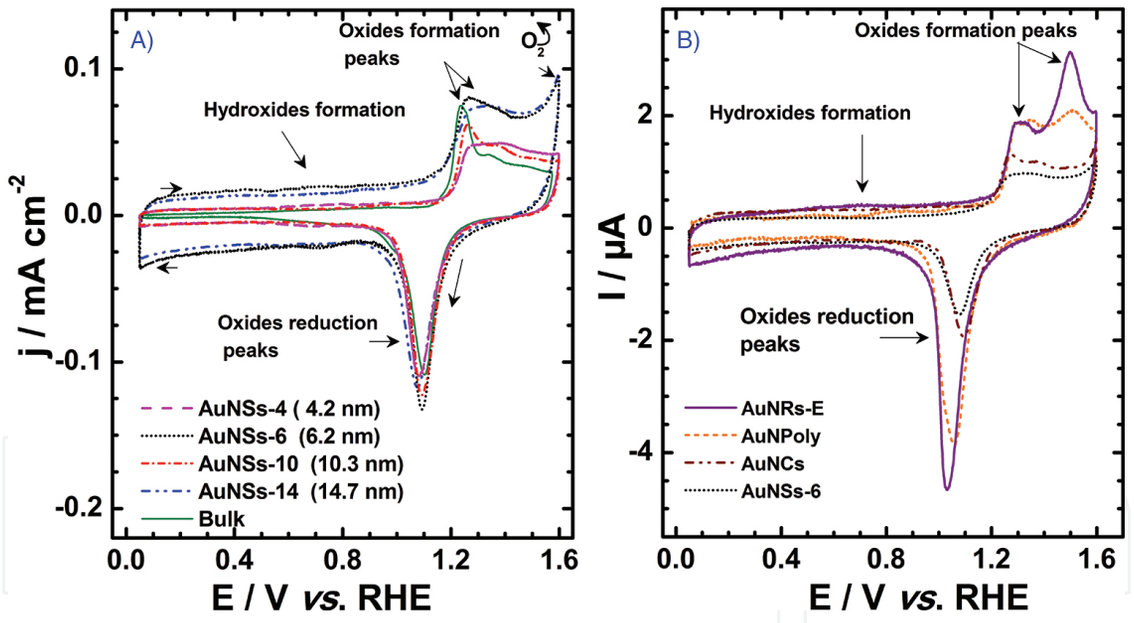

Figure 5. Cyclic voltammograms of the: (A) gold bulk and the different spherical AuNPs (AuNSs-4, AuNSs-6, AuNSs-10, and AuNSs-14); (B) shape controlled AuNPs (AuNSs, AuNRs, AuNCs, and AuNPoly) electrodes in 0.1 mol L^{-1} NaOH, recorded at 20 mV s^{-1} and at controlled temperature of 20°C. (A) Reprinted and adapted with permission from Ref. [3]; Copyright 2016, John Wiley & Sons, Inc. (B) Reprinted and adapted with permission from Ref. [4]; Copyright © 2013, The Author(s).

At higher potentials than 1.2 V vs. RHE, different oxidation peaks depending on the particles shape can be noticed: one oxidation peak is observed for spherical gold nanoparticles at 1.25 V vs. RHE (**Figure 5A**); two peaks are revealed on the surface of AuNRs and polyhedral particles at 1.25 V and 1.35 V vs. RHE, respectively (**Figure 5B**), and one main oxidation peak

http://dx.doi.org/10.5772/64770

is observed at 1.25 V followed by shoulder peaks between 1.35 V and 1.50 V vs. RHE for bulk gold electrode. AuNCs also exhibits two oxidation peaks located at 1.15 V and 1.25 V vs. RHE. The peak which maximum centered around 1.2 V vs. RHE is typical contribution of (1 1 1) plans. The nature of the oxides formed depends on the structure of the electrode. Most of the authors refer to the formation of higher oxides from the following equation (Eq. (1)) [53, 54].

$$Au.H_2O + 3HO^- \rightarrow Au(OH)_3 + H_2O + 3e^- \quad (1)$$

During the backward potential scan, such oxides are reduced irreversibly from 1.4 to 0.8 V vs. RHE.

Interestingly, the particle morphology affects the profile of the double layer and oxides formation regions strongly. Indeed, the increase in size of gold particles diameter from 4 nm to the bulk leads to a thin double layer and well-defined oxide region on the CVs. Such features in the change of the CV profile indicate the increase in metallic trend as a function of the particle size. Additionally, small AuNSs (14.7 ± 2.9 and 6.2 ± 1.2 nm) exhibit high affinity with oxygen species, which is revealed by the oxygen evolution reaction observed at ca. 1.60 V vs. RHE, that is, an electrode potential lower than that on the bulk material [3].

3.2. Under-potential deposition of lead adatoms in alkaline solution

The under-potential deposition (UPD) of adatoms on noble metals such as platinum or gold is also a helpful tool for characterizing the surface structure of electrode materials [55, 56]. In general, it involves the deposition of up to one monolayer of metal on a foreign substrate at potentials higher to the reversible thermodynamic potential. The positive overpotential at which this process occurs is considered to be a direct consequence of the high bonding energy of the metal being deposited at the substrate surface. It has been previously shown that the synthesis method affects the crystallographic structure of AuNPs [36, 55–57]. Because of its high sensitivity with the gold surface, the UPD of lead (Pb_{UPD}) was employed to characterize the crystallographic structure of the synthesized spherical AuNPs [3–5, 16, 56]. **Figure 6** shows Pb_{UPD} on bulk and AuNPs in 0.1 mol L^{-1} NaOH + 1 mmol L^{-1} $Pb(NO_3)_2$ at 20 mV s^{-1}. During the negative potential scan from 0.85 to 0.25 V vs. RHE on the bulk gold electrode, three reduction peaks assigned to the deposition of lead on (1 1 0), (1 0 0), and (1 1 1) facets were observed around 0.52, 0.44 and 0.39 V vs. RHE, respectively. During the positive potential scan, three stripping peaks corresponding to the reversible desorption and dissolution of Pb layer on (1 1 1), (1 0 0), and (1 1 0) facets were observed around 0.42, 0.47, and 0.58 V, respectively. For the AuNSs materials (**Figure 6**), no desorption peak of lead on (1 0 0) facet was observed for the small AuNSs-4 (4.2 ± 0.7 nm), AuNSs-6 (6.2 ± 1.2 nm), and AuNSs-10 (10.3 ± 1.4 nm). However, an increase in the particle size leads to a formation of (1 0 0) facets for the large particles such as AuNSs-14. These results clearly show that the surface properties can be perfectly modeled by tailoring the particle size. The Pb_{UPD} on the shape controlled AuNPs has been extensively discussed in our previous works [4, 5]. Until now, the Pb_{UPD} permitted to reveal only the low-index facets. Investigations on high-index facets are needed.

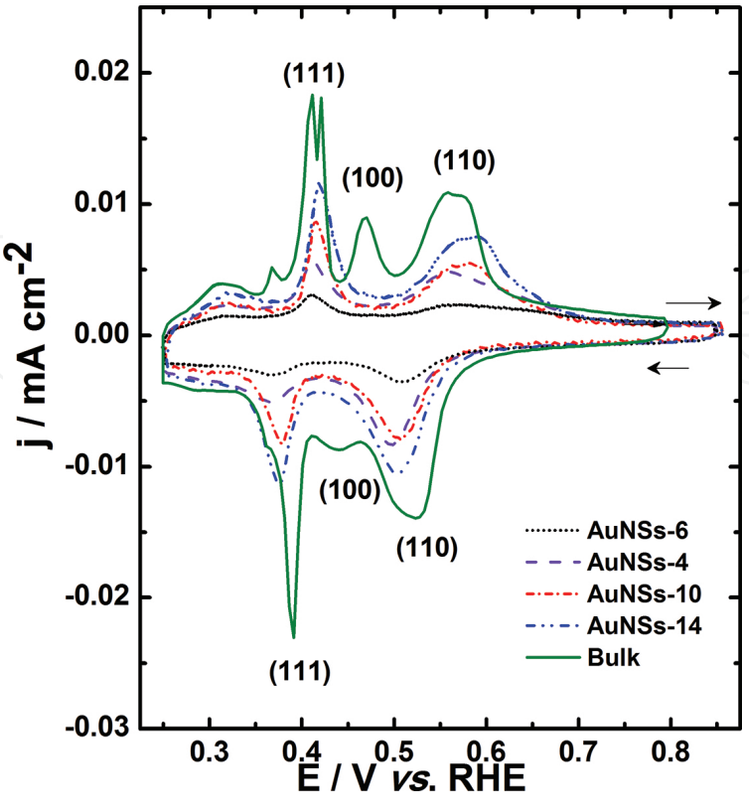

Figure 6. Voltammetric UPD profiles of the different: spherical AuNPs and bulk in 0.1 mol L^{-1} NaOH + 1 mmol L^{-1} $Pb(NO_3)_2$ recorded at 20 mV s^{-1} and at controlled temperature of 20°C. Reprinted and adapted with permission from Ref. [3]; Copyright 2016, John Wiley & Sons, Inc.

4. Glucose electrooxidation on gold-based catalysts

Carbohydrate-based energy converters are emerging as unavoidable powerful, durable, cheap, and environmentally friendly items. In addition, the selective electrochemical conversion of these highly functionalized organic molecules (glucose, lactose, etc.) may offer valuable benefits such as electricity, heat, and added-value chemicals. The total glucose electrooxidation involves 24 electrons per molecule and enables getting an open circuit voltage of 1.25 V, which represents a free energy of 2871 kJ mol^{-1}, that is, 4.430 kWh kg^{-1} [58]. For 2-electron process, it yields 1.43 V at pH = 13, that is, a specific energy of 0.435 kWh kg^{-1}. Gluconate is a high added-value product, and its derivatives, such as gluconolactone or sodium and calcium salts, are used in food, pharmaceutical, and cosmetic industries [59]. The effective development of efficient fuel cells relies on the kinetics of both reactions at the cathode and anode. Indeed, the anode catalyst must withstand the hard poisoning phenomenon due to strongly adsorbed intermediates. Up to now, glucose electrooxidation at the anode, or even with the most active nanocatalyst (Pt), largely occurs with overpotential ≥200 mV. Theoretically, at pH 13, glucose electrooxidation must start at −0.24 V vs. RHE [51]. Unfortunately, Pt the most dehydrogenation catalyst is rapidly deactivated. The best compromise relies on gold-based materials, which play a crucial role in the catalysis of hemiacetal compounds resulting in

http://dx.doi.org/10.5772/64770

enhanced intrinsic activity and reaction turnover. The capability of gold in oxidizing carbohydrates can be tuned through its size and morphology during its synthesis. The following sections focus on the recent efforts that have been devoted for engineering advanced electrode materials, which can offer a great opportunity of achieving enhanced catalytic performances.

4.1. Size effect: case of spherical gold nanoparticles

The assessment of the determining parameters that influence the activity of catalysts is of paramount interest in electrocatalysis. **Figure 7** highlights the effect of the particles size on the catalytic properties of the unsupported-gold electrode materials for the glucose oxidation in alkaline solution.

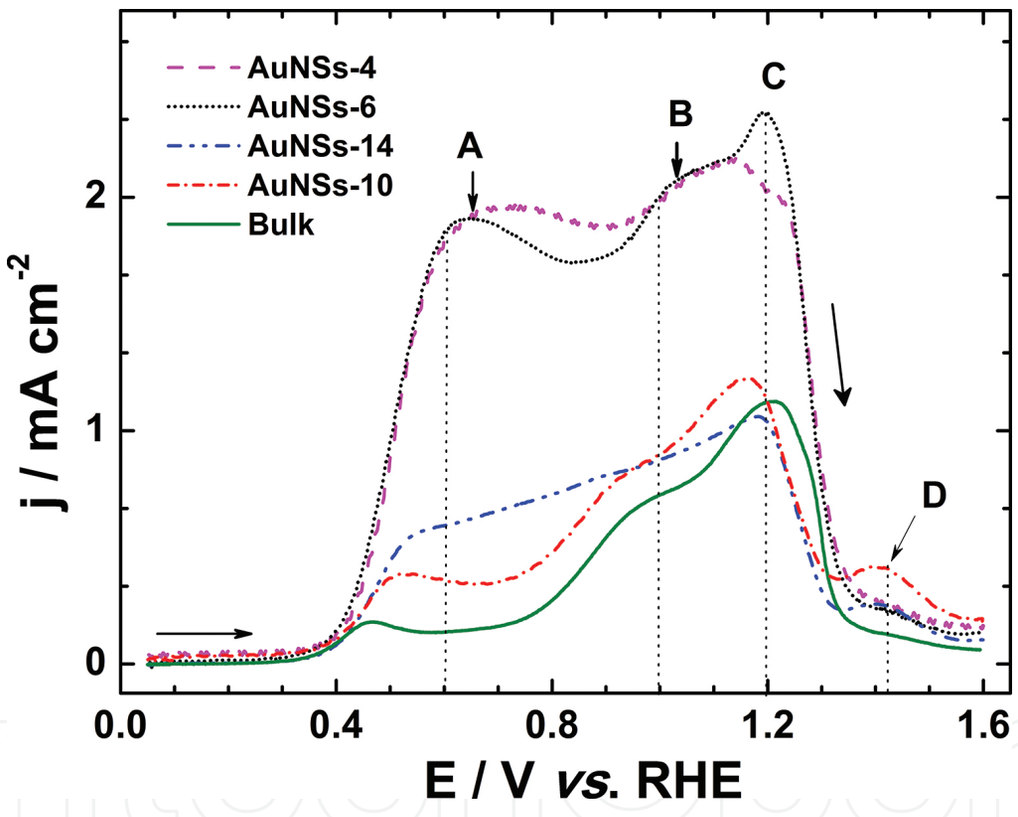

Figure 7. (A) Positive scan of the voltammograms of the gold bulk and the different AuNSs (AuNSs-4, AuNSs-6, AuNSs-10, and AuNSs-14) electrodes in 0.1 mol L^{-1} NaOH + 10 mmol L^{-1} glucose recorded at 20 mV s^{-1} and at controlled temperature of 20°C. Reprinted and adapted with permission from Ref. [3]; Copyright 2016, John Wiley & Sons, Inc.

On AuNSs-4, the oxidation of glucose begins at ca. 0.35 V vs. RHE followed by three oxidation peaks. The first one centered at 0.60 V is a broad oxidation peak (peak A) which maximum reaches $j_{max} = 2$ mA cm^{-2} and assigned to the dehydrogenation of the anomeric carbon of glucose in C1-position leading to the formation of gluconolactone as intermediate or final product [1, 2, 60, 61]. The second peak (B) centered at 1.00 V vs. RHE may correspond to the oxidation of adsorbed intermediates followed by the main oxidation peak at 1.20 V vs. RHE

(peak C) as previously observed for other AuNPs, single or polycrystalline gold electrodes [2, 4, 5, 62, 63]. According to the literature, several products such as gluconate or glucuronate can be resulted in the electrochemical oxidation of the glucose molecule at the Au oxide/hydroxide species, gluconate being issued from hydrolysis of the lactone in the bulk solution [1, 2, 61, 62, 64]. Nanospheres having average size of 4.2 and 6.2 nm (AuNSs-4 and AuNSs-6) display similar electroactivities despite the slight difference in size due to the large presence of (1 1 0) facets for AuNSs-6 compared to AuNSs-4. The effect of the crystallographic structure will describe in details in the next section.

The current density corresponding to the dehydrogenation process of the glucose molecule (peak A) is 3.2-, 4.9-, and 11.0-fold higher for AuNSs-4 than those observed for AuNSs-10, AuNS-20, and the bulk electrode, respectively. Similar comparison shows current densities, respectively, for the same AuNSs, 2.0-, 2.2-, and 2.1-fold higher than the bulk gold electrode toward glucose oxidation at peak C.

Based on both the CV results, it can be concluded that the electrocatalytic activities of the different spherical gold electrodes toward glucose oxidation are size and structure dependent. The formation of $(OH)_{ads}$ on Au is crucial for the electrochemical oxidation of glucose [60]. Thereby, the oxidation of glucose is assumed to occur through the interaction between the adsorbed hemiacetal group and $(OH)_{ads}$. It is generally accepted that the AuOH sites on the Au surface act as the active species for glucose oxidation [65]. Therefore, the oxidation of glucose strongly depends on the number of AuOH sites. The first step of the oxidation of glucose in alkaline media involves the adsorption of glucose on Au surface through the anomeric carbon leading to the dehydrogenation process *via* the formation of an adsorbed radical. This process leads to the formation of gluconolactone [62, 64]. Furthermore, gluconolactone can be hydrolyzed in solution to give sodium gluconate or the gluconolactone adsorbates can interact with the metal center represented by these AuOH species to give more than two-electron oxidation products resulting from carbon-carbon bond cleavage [60, 65]. The second step deals with the oxidation of adsorbed intermediates or gluconolactone with the adsorbed OH species. Several products can be obtained as indicated in the literature [62].

4.2. Morphology effect

The electrooxidation of glucose has intensively been studied on gold single crystals and gold nanoparticles in the 1990s [2, 60, 64, 66]. More recently, we have investigated the dependence of the activity on low-index crystalline surface of AuNPs toward the glucose oxidation [4, 5]. At this stage of our investigations, electrocatalytic activity of AuNPs is sensitive to their morphology [2, 67]. It was mentioned that the oxidation of the glucose depends on the surface structures that determine the adsorbed intermediates [2, 4, 5, 64]. It was concluded that the glucose oxidative conversion is enhanced according to the crystallographic orientation of the electrocatalyst as follows: (1 0 0) > (1 1 0) > (1 1 1).

Figure 8 shows the positive potential going profile of different AuNPs recorded during the glucose oxidation. This reaction begins at ca 0.3 V vs. RHE for all materials followed by the first oxidation peak, which is associated with the formation of gluconolactone species. Surprisingly, AuNSs (dot line) and AuNCs (dashed dot line) show high activities for the

http://dx.doi.org/10.5772/64770

oxidation of glucose. This sharp oxidation peak appears at 0.54 V vs. RHE for AuNCs, 100 mV lower than for AuNSs. Afterwards, the oxidation covers a large potential range from 0.8 to 1.3 V vs. RHE. AuNRs (solid line) and AuNPolys (dashed line) show an overlap shoulder followed by a maximum oxidation peak at 1.3 V vs. RHE. However, this peak is observed at 1.2 V vs. RHE for AuNSs and AuNCs. The high current density observed for AuNSs can be related to their small size (around 6 ± 2 nm) and their electronic surface structure. The catalytic effect on AuNCs depends on their structure, that is, the number of sites of low coordination. AuNCs exhibit the mean (1 0 0) and (1 1 0) facets that promote dehydrogenation of the molecule of glucose at low potential (0.54 V vs. RHE) compared to the other nanostructured materials. These facets are the most favorable for this reaction [64]. According to theoretical model developed by Hammer and Nørskov [68], and Bell et al. [69], the d-band of the orbital plays an essential role in the adsorption of reactants and intermediates on metal surfaces. As suggested, the d-orbital occupancy reflects the number of electrons available to participate in bonding between the metal center and the adsorbate. However, all these explanations do not elucidate the similar activity between the AuNSs and AuNCs whose surface structures are theoretically different. Consequently, more investigations combining different techniques are certainly required.

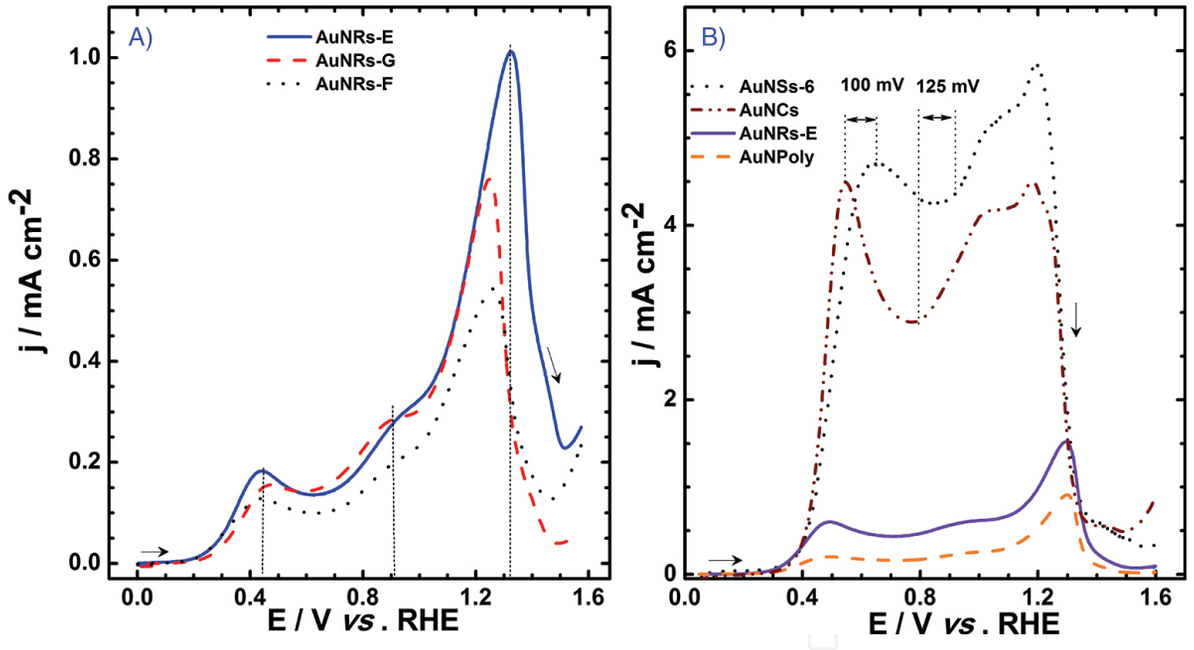

Figure 8. Positive scan of voltammograms of the different AuNPs: (A) AuNRs-E, AuNRs-F, and AuNRs-G; (B) AuNSs-6, AuNRs-E, AuNCs, and AuNPoly electrodes in 0.1 mol L^{-1} NaOH + 10 mmol L^{-1} glucose recorded at 20 mV s^{-1} and at controlled temperature of 20°C. (A) Reprinted and adapted with permission from Ref. [3]; Copyright 2016, John Wiley & Sons, Inc. (B) Reprinted and adapted with permission from Ref. [4]; Copyright © 2013, The Author(s).

4.3. Support effect: performances of carbon supported gold nanoparticles

The direct immobilization of metal NPs onto carbon-based substrates induces a high improvement in their catalytic performances, assigned to better interaction between NPs and the

support [70, 71]. In addition, a support is needed to boost the current in real application such FCs. Free NPs in solution are used to find out the intrinsic activity of the catalysts, especially the structure sensitivity [70]. Thus, single crystals and shape-controlled NPs constitute cornerstones for the fundamental understanding of the catalytic activity and carbon-supported NPs serve as subgrades for practical use. The electrochemical behavior of different carbon-based Au electrodes is shown in **Figure 9** in the absence and presence of glucose in alkaline medium. Considering the supporting electrolyte, there is no obvious evidence of Au in the case of Au@CFs despite the loading of 26 wt.% (**Figure 9A**). Contrariwise, two major features during the positive scan (A′: metal oxidation) and the negative scan (C′: oxide reduction) typify gold at Au nanocorals (**Figure 9B**) and Au/C (**Figure 9C**) electrodes. However, all electrodes show activity toward glucose electrooxidation, marked by several peaks during the forward (glucose dehydrogenation, oxidation) and only one main peak in backward. The reaction starts at ca. −0.5, −0.4, and −0.6 V vs. Ag|AgCl (at pH 13, $Ag|AgCl|KCl_{sat}$ = +0.96 V vs. RHE) on Au@CFs, Au nanocorals and Au/C, respectively. Otherwise, Au/C shows improved kinetics with ca. 100 mV shift toward lower potentials, which is auspicious for application as anode material. Furthermore, the coincidence of the peak labeled by "C1" in **Figure 9C** during the negative scan with the gold oxides reduction one indicates that the main phenomenon concerns the oxidation of new glucose molecules at the freshly released Au active sites. By taking into account Au content and the electrolyte composition (see caption), Au/C exhibits the best performance. Indeed, the Au nanocoral electrode has 35-fold higher Au content than Au/C. Furthermore, among the nanostructures obtained by the electrodeposition (see **Figure 3**), Au nanocorals exhibit the best electrocatalytic activity that is 1.54- and 2.2-fold higher than AuNPs and the sputtered Au film electrodes, respectively [44]. This has been ascribed to its structure, especially the presence of Au(1 1 0) facets [43, 44].

To better evaluate the ability of these electrodes, some direct glucose fuel cell (DGFC) tests have been performed. **Figure 10A** and **B** displays the DGFC performances using the electrochemically grown Au nanostructures on carbon paper as anode materials [44]. The open-circuit voltage (OCV) is 0.45, 0.61, and 0.64 V for sputtered film, nanoparticles, and nanocorals, respectively. The achieved maximum output power density (P_{max}) is 0.12, 0.34, and 0.85 mW cm^{-2} for the same sequence. This tendency, in agreement with the CV data, can be explained by the high surface area of Au nanocorals electrode and definitely, its structure that may better facilitate the diffusion of the species. This is supported by AuNPs electrode where the ohmic drop (IR) is more significant than its Au nanocorals counterpart with similar OCV. Among the three electrodes, the sputtered film is certainly the densest, which explained the inaccessibility to some actives sites and hard mass transport phenomenon. **Figure 10C** presents the DGFC performances at different concentrations of glucose using Au/C synthesized from the BAE method as anode material [51]. The OCV is quite similar, 0.90V (±20 mV); P_{max} = 0.86 (0.1 M), 1.43 (0.2 M), 2.02 (0.3 M), and 1.52 mW cm^{-2} (0.4 M). The achieved P_{max} value of 2.02 mW cm^{-2} for 0.3 M glucose with 0.18 mg_{Au} cm^{-2} at 25°C surpasses (> two-fold) the reported data, for example, 1.08 mW cm^{-2} (1.2 mg_{PtRu} cm^{-2}) [72], 0.52 mW cm^{-2} (0.45 mg_{AuPtPd} cm^{-2}) [73], and 1.1 mW cm^{-2} (0.6 mg_{Au} cm^{-2}) [74]. In addition, it outperforms the previous results from the electrodeposition method [44]. Importantly, a record OCV of 1.1 V has been reached in 0.5 M

NaOH using Au/C from BAE as anode [51]. In conclusion, the BAE method foreshadows good prospects for the development of efficient anode materials.

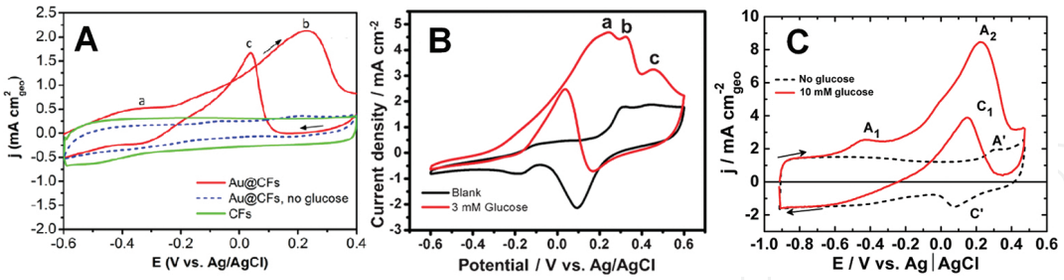

Figure 9. CVs recorded at 50 mV s^{-1} for evaluating the electrocatalytic activity of different Au-based electrodes. (A) AuNPs embedded in electrospun CFs (0.1 mol L^{-1} KOH, 10 mmol L^{-1} glucose, Au content = 26 wt.%). (B) Electrochemically grown Au nanocorals on carbon paper (0.5 mol L^{-1} KOH, 3 mmol L^{-1} glucose, Au loading = 2743 μg cm^{-2}). (C) AuNPs dispersed on Vulcan XC 72R carbon (20 wt.% Au/C, from BAE method) and then deposited onto a glassy carbon electrode (0.1 mol L^{-1} NaOH, 10 mmol L^{-1} glucose, Au loading = 78 μg cm^{-2}). (A) Reprinted and adapted with permission from Ref. [42]; Copyright 2016, John Wiley & Sons, Inc. (B) Reprinted and adapted with permission from Ref. [44]; Copyright 2012, RSC. (C) Reprinted and adapted with permission from Ref. [51]; Copyright 2016, John Wiley & Sons, Inc.

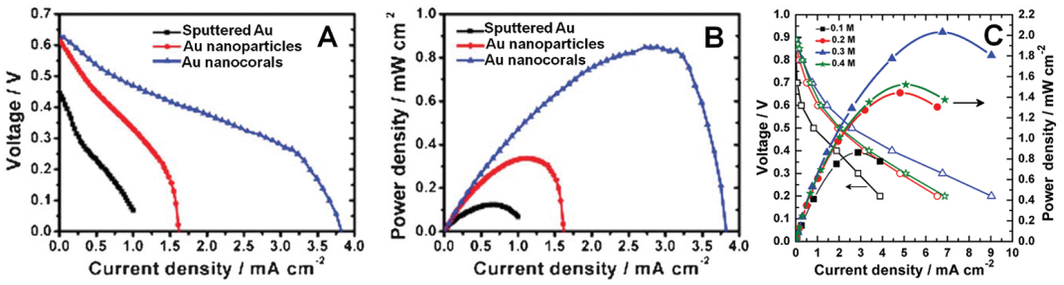

Figure 10. (**A** and **B**) Plots of direct glucose fuel cell performances in terms of **(A)** Cell voltage and **(B)** power density, from the electrochemically grown Au nanostructures on carbon paper as anode (electrode of 1 cm^2, Au loading = ~2.7 mg cm^{-2}; deaerated solution of 0.5 M KOH + 0.3 M glucose) and Pt cathode (metal loading not available, O_2-saturated 0.5 M KOH solution). **(C)** Direct glucose fuel cell polarization curves for different concentrations of glucose: cell voltage (left *Y*-axis) and power density (right *Y*-axis) from Au/C synthesized from the BAE method as anode (electrode of 2 cm^2, Au loading = 0.18 mg cm^{-2}; deaerated solution of 0.5 M KOH + glucose). Pt synthesized from the BAE method was used as cathode (electrode of 2 cm^2, Pt loading = 0.17 mg cm^{-2}; O_2-saturated 0.5 KOH). (**A**, **B**) Reprinted and adapted with permission from Ref. [44]; Copyright 2012, RSC. **(C)** Reprinted and adapted with permission from Ref. [51]; Copyright 2016, John Wiley & Sons, Inc.

5. Reaction intermediates/products from glucose electrooxidation

5.1. Spectroelectrochemical investigations on AuNPs

Coupling electrochemistry to spectroscopy enables better understanding of the challenging anodic reaction. Mostly, *in situ* spectroelectrochemical experiments consist of coupling either cyclic voltammetry to FTIRS (CV-FTIRS or SPAIRS) or chronoamperometry to FTIRS (CA-

FTIRS) [47]. For the mechanistic purpose, the *in situ* FTIRS in its Single Potential Alteration Infrared Reflectance (SPAIR) variant was undertaken to study the glucose electrooxidation on gold nanoparticles in alkaline medium [3, 47, 75]. This study enables the identification of adsorbed reaction intermediates and/or the final products. **Figure 11** shows the SPAIR spectra obtained for spherical gold catalysts during the glucose electrooxidation reaction.

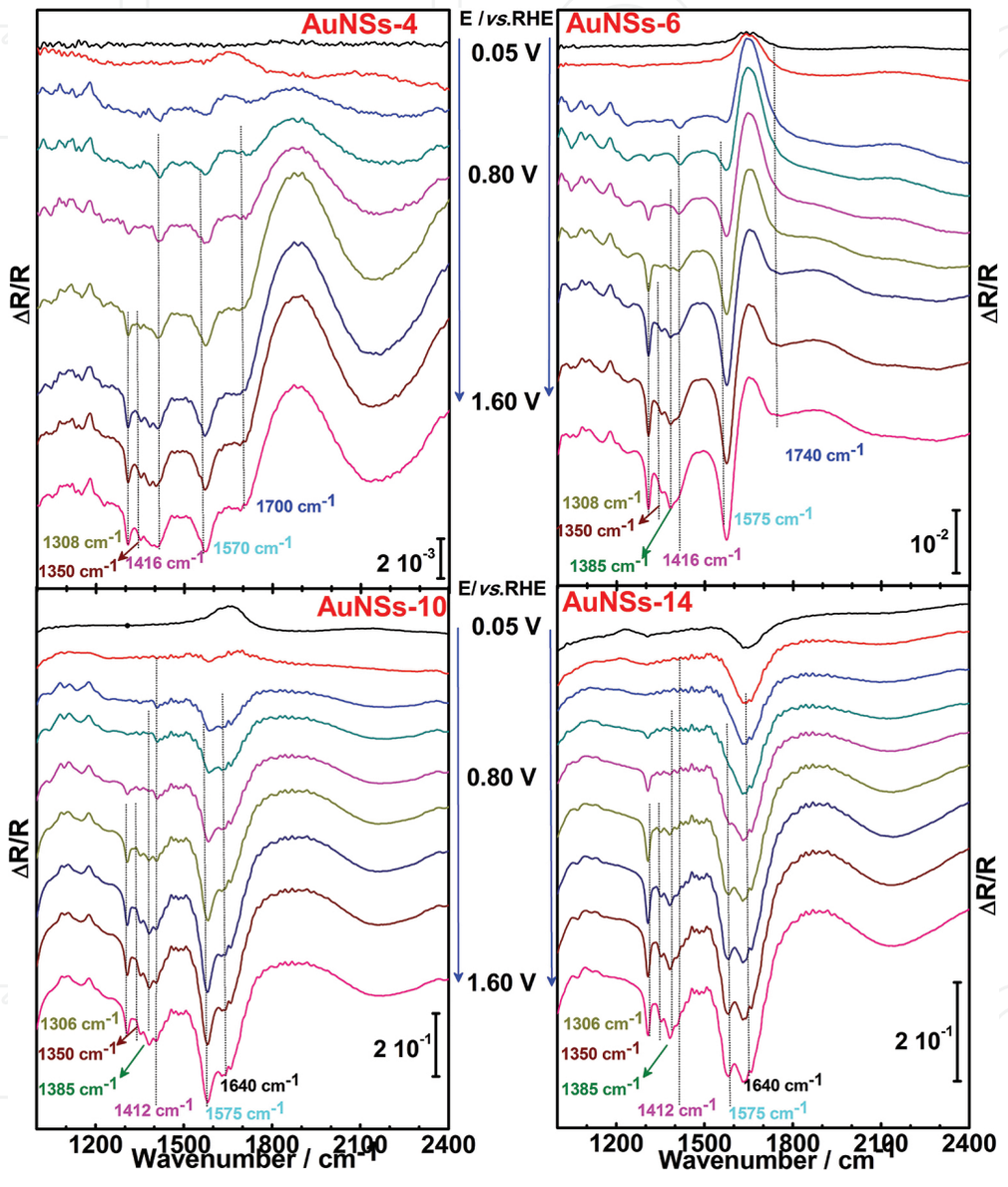

Figure 11. SPAIR spectra recorded in 0.1 mol L^{-1} NaOH electrolyte containing 10 mmol L^{-1} of D-(+)-glucose at 1 mV s^{-1} on AuNSs-4, AuNSs-6, AuNSs-10, and AuNSs-14 electrocatalysts in the potential domain 0.05–1.6 V vs. RHE. Reprinted and adapted with permission from Ref. [3]; Copyright 2016, John Wiley & Sons, Inc.

From the SPAIRS spectra, the presence of gluconate is revealed by the three down-going vibration bands at 1350, 1416, and ca. 1575 cm^{-1} [3] corresponding, respectively, to CH_2 deformation, O—C—O symmetric, and asymmetric stretchings of this compound. The band at 1732 cm^{-1} together with the small band at ca. 1385 cm^{-1} is assigned to the C═O stretching

and CH_2 deformation $\delta(CH_2)$ vibration modes of δ-gluconolactone [61, 76]. In addition, the formation of gluconate occurs on the full range of potential, that is, from ca. 0.2 to 1.6 V vs. RHE as well as during the backward potential scan. Furthermore, the presence of the adsorbed reaction intermediate (δ-gluconolactone) on the electrode surface was confirmed by a slight downshift of the ν(C═O) band to lower wave numbers. δ-Gluconolactone is the primary reaction product of the glucose oxidation. After it desorption from the electrode surface, the lactone diffuses into solution and its cyclic structure becomes carboxylate anion after its electrolysis. The main product after this process is the gluconate. Finally, the feature vibration band of oxalate was identified through a sharp band at 1308 cm^{-1} which indicated a C—C bond cleavage of gluconate, as already reported [77]. Therefore, AuNSs electrode materials prepared herein are the best to convert glucose into gluconate *via* its corresponding δ-lactone in alkaline medium; the further dissociative adsorption of this main product at the electrode surface results in a C—C bond cleavage of the initial six-carbon molecule skeleton.

5.2. (Electro)Analytical investigations

Organic chemistry that consists of breaking and coupling various chemical bonds, for example, C—C, C—H, C—N, C—O, etc., enables the total synthesis of wide range of organic molecules and indirectly involves electron-transfer-driven reactions. Thus, electrochemical methods could serve as straightforward and powerful routes that could inspire the development of numerous elegant approaches to produce chemicals from C—C coupling reactions, functional-group interconversion, and installation of heteroatom moieties [78, 79]. Otherwise, organic electrosynthesis replaces toxic or hazardous reagents, avoids large quantities of stoichiometric oxidants and reductive reagents, and can be used for the *in situ* production of unstable and hazardous reagents [80]. Consequently, the waste originating from the reagents used is almost negligible since only an unconsumed and recyclable electrode material and electrical current serve as reagents. Thus, electrochemistry complies with all the criteria of "green chemistry" [79, 80]. One of the keys of the major gate leading to such breakthroughs is the electrode material that must exhibit high selectivity. Metal nanomaterials from BAE method have been used as electrodes for the electrochemical conversion of carbohydrates using glucose, galactose, and lactose as models [51].

The high-performance liquid ionic chromatographic (HPLIC) analysis of the sample after electrolysis at Au/C (BAE method) is depicted in **Figure 12A** and highlights the presence of two unresolved peaks at t_R = 5.5 and 6.1 min, assigned to gluconate. Importantly, the combination of *in situ* FTIRS and HPLIC unambiguously state that C—C bond cleavage does not occur, which highlights the high selectivity of the electrode material [51]. The inset shows the time-dependent experimental number of electrons (n_{exp}) and subsequently the experimental Faradaic yield (τ_F). After 7.5 h of electrolysis, n_{exp} = 2.05 and τ_F = 102%. It was demonstrated that the catalyst efficiency was nearly 90% [51], which illustrates the excellent capability of Au/C to overcome the deactivation phenomena and oxidize selectively most of the carbohydrates at the C1-position in two-electron process. To validate previous results, analytical determination of the reaction products by liquid chromatography coupled with mass spectrometry (LC-MS) was performed. **Figure 12B** shows the spectrum of the sample from

glucose electrolysis and after resin exchange (H^+-exchange) neutralization followed by lyophilization to generate the acid form of the reaction products. It displays a major peak at m/z = 195 that belongs to the pseudo-molecular ions $(M–H)^-$ of gluconic acid, whereas those at m/z = 129 and 391 are attributed to the fragmentation and simple dimerization processes. The ^{13}C NMR spectrum of the sample is displayed in **Figure 12C**. The ^{13}C chemical shifts of 95.9 and 92 ppm are assigned to the carbon at C1-position of the β-glucose and α-glucose (unreacted) and those at 176.9, 175.8, and 173.6 ppm as attributed to C1-position of gluconic acid, γ-gluconolactone and δ-gluconolactone [51]. More importantly, the spectrum of the lyophilized gluconic acid solution (commercial) and that of gluconate (commercial) after H^+-exchange and lyophilization are identical to the electrolysis sample. Consequently, the electrooxidation of carbohydrates at this Au/C concerns exclusively the carbon at C1-position and involves two electrons, thus underpinning the conclusion that the electrocatalysis can be used to oxidize selectively carbohydrates. This fundamental understanding of glucose oxidation taken as model can enable an efficient design of high-output-power co-generation devices for the energy and chemicals production from selective oxidation of the anomeric carbon of glucose and its related carbohydrates without any restrictive function protection.

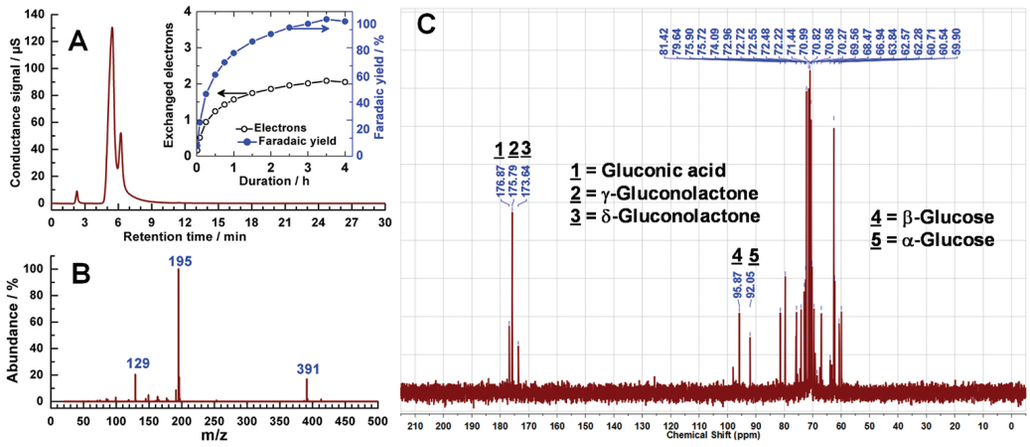

Figure 12. (Electro)Analytical investigations of the reaction products from the electrolysis in 0.1 M NaOH at 0.8 V vs. RHE using an electrode composed of 20 wt.% Au/C nanocatalyst synthesized from the BAE method. (A) HPLIC chromatograms from the electrolysis of 20 mM glucose: the inset shows the experimental exchanged number of electrons (left *Y*-axis, black) and experimental Faradaic yield (right *Y*-axis, blue) based on the electrolysis of 50 mM glucose. (B) LC-MS-negative ionization mass spectrum (M-1) of the product. (C) ^{13}C NMR spectrum from the electrolysis of 20 mM glucose. Reprinted and adapted with permission from Ref. [51]; Copyright 2016, John Wiley & Sons, Inc.

6. Concluding remarks

Wet chemical methods are most versatile and highly flexible to synthesize size and shape controlled gold nanoparticles. From a fundamental point of view, the growth kinetic of nanomaterials constitutes a very important field of study in the understanding and designing of catalysts. This chapter explained nanocrystals growth. It also shows the main role of such studies in the development of new synthesis routes. The dependence of diameter and the

form of the size distribution in the reaction-limited regime were well demonstrated. It is observed that the growth of nanocrystals can be controlled either by diffusion or by the reaction at the surface.

Such size control processes enable the synthesis of nanoparticles with good size distribution and well-defined surface structure allowing electrocatalytic reactions with good reactivity and selectivity. Transmission electron microscopy images and the electrochemical characterization through the sensitive method of UPD of lead allowed to analyze extensively the surface orientation of different gold nanomaterials. It was found that the as-prepared gold nanomaterials are structurally composed of (1 1 1), (1 1 0), and (1 0 0) index facets.

The electrocatalytic activity of different AuNPs was elucidated. It was shown that AuNPs exhibited high electrochemical activity toward glucose oxidation in alkaline medium. The correlation of the physical/electrochemical characterizations leads to show that the glucose electrooxidation is a size, shape, and crystallographic structure sensitive reaction. Small spherical gold with mean diameter of 4.2 nm shows higher performance to this reaction than counterparts. The small particles induced an increase in surface electronic effect, which enhanced the catalytic activity. In contrast, (1 0 0) facet appeared as the more active facet by improving the catalytic activity of the materials.

The main reaction product of the glucose electrooxidation was identified by *in situ* infrared spectroscopy. It revealed that the adsorption of the reactant started by dehydrogenation of the molecule to δ-gluconolactone. Further analytical investigations with *ex situ* techniques such as LC-MS and NMR permitted to assess gluconic acid as the main reaction product..

Author details

Seydou Hebié, Yaovi Holade, Karine Servat, Boniface K. Kokoh and Têko W. Napporn*

*Address all correspondence to: Teko.napporn@univ-poitiers.fr

IC2MP, UMR 7285 CNRS, University of Poitiers, Poitiers, France

References

[1] Hsiao MW, Adzic RR, Yeager EB. The effects of adsorbed anions on the oxidation of d-glucose on gold single crystal electrodes. Electrochimica Acta. 1992;37:357–363. doi: http://dx.doi.org/10.1016/0013-4686(92)85024–F.

[2] Wang J, Gong J, Xiong Y, Yang J, Gao Y, Liu Y, Lu X, Tang Z. Shape-dependent electrocatalytic activity of monodispersed gold nanocrystals toward glucose oxidation. Chemical Communications. 2011;47:6894–6896. doi:10.1039/C1CC11784J.

[3] Hebié S, Napporn TW, Morais C, Kokoh KB. Size-dependent electrocatalytic activity of free gold nanoparticles for the glucose oxidation reaction. ChemPhysChem. 2016;17:1–10. doi:10.1002/cphc.201600065.

[4] Hebié S, Kokoh KB, Servat K, Napporn T. Shape-dependent electrocatalytic activity of free gold nanoparticles toward glucose oxidation. Gold Bulletin. 2013;46:311–318. doi: 10.1007/s13404-013-0119-4.

[5] Hebié S, Cornu L, Napporn TW, Rousseau J, Kokoh BK. Insight on the surface structure effect of free gold nanorods on glucose electrooxidation. The Journal of Physical Chemistry C. vol. 117 (19), 2013:9872–9880. doi:10.1021/jp401009r.

[6] LaMer VK, Dinegar RH. Theory, production and mechanism of formation of monodispersed hydrosols. Journal of the American Chemical Society. 1950;72:4847–4854. doi:10.1021/ja01167a001.

[7] R. Viswanatha, D. D. Sarma, Growth of Nanocrystals in Solution. In Nanomaterials Chemistry; C. N. R. Rao, A. Mller, A. K. Cheetham, Eds.; WileyVCH Verlag GmbH & Co. KGaA: Weinheim, Germany, p139–170, 2007.

[8] Talapin DV, Rogach AL, Haase M, Weller H. Evolution of an ensemble of nanoparticles in a colloidal solution: theoretical study. The Journal of Physical Chemistry B. 2001;105:12278–12285. doi:10.1021/jp012229m.

[9] Lifshitz IM, Slyozov VV. The kinetics of precipitation from supersaturated solid solutions. Journal of Physics and Chemistry of Solids. 1961;19:35–50. doi: http://dx.doi.org/10.1016/0022-3697(61)90054–3.

[10] C. Wagner. Theorie der alterung von niederschlagen durch umlosen (ostwald–reifung). Z. Elektrochem., 65:581–591, 1961.

[11] WZ Ostwald. Blocking of ostwald ripening allowing long–term stabilization. Zeitschrift für physikalische Chemie, p37:385, 1901.

[12] Frens G. Particle size and sol stability in metal colloids. Kolloid-Zeitschrift und Zeitschrift für Polymere. 1972;250:736–741. doi:10.1007/bf01498565.

[13] Turkevich J, Stevenson PC, Hillier J. A study of the nucleation and growth processes in the synthesis of colloidal gold. Discussions of the Faraday Society. 1951;11:55–75. doi:10.1039/df9511100055.

[14] Brust M, Walker M, Bethell D, Schiffrin DJ, Whyman R. Synthesis of thiol-derivatised gold nanoparticles in a two-phase Liquid-Liquid system. Journal of the Chemical Society, Chemical Communications. 1994:801–802. doi:10.1039/c39940000801.

[15] Slot JW, Geuze HJ. A new method of preparing gold probes for multiple-labeling cytochemistry. European Journal of Cell Biology. 1985;38:87–93.

[16] Habrioux A, Hebié S, Napporn T, Rousseau J, Servat K, Kokoh KB. One-step synthesis of clean and size-controlled gold electrocatalysts: modeling by taguchi design of experiments. Electrocatalysis. 2011;2:279–284. doi:10.1007/s12678-011-0064-z.

[17] Trouiller AJ, Hebié S, el Bahhaj F, Napporn TW, Bertrand P. Chemistry for oncotheranostic gold nanoparticles. European Journal of Medicinal Chemistry. 2015;99:92–112. doi: http://dx.doi.org/10.1016/j.ejmech.2015.05.024.

[18] Pradel Tonda-Mikiela, T. W. Napporn, Cláudia Morais, Karine Servat, Aicheng Chen, Kokoh. B. Synthesis of gold-platinum nanomaterials using bromide anion exchange-synergistic electroactivity toward CO and glucose oxidation. Journal of the Electrochemical Society. 2012;159: H828–H833. doi:10.1149/2.001211jes.

[19] Sun J, Guan M, Shang T, Gao C, Xu Z, Zhu J. Selective synthesis of gold cuboid and decahedral nanoparticles regulated and controlled by Cu^{2+} ions. Crystal Growth & Design. 2008;8:906–910. doi:10.1021/cg070635a.

[20] Wang ZL. Characterization of nanophase materials. Wiley, New-York, NY, 2000.

[21] Jana NR, Gearheart L, Murphy CJ. Wet chemical synthesis of high aspect ratio cylindrical gold nanorods. The Journal of Physical Chemistry B. 2001;105:4065–4067. doi:10.1021/jp0107964.

[22] Jana NR, Gearheart L, Murphy CJ. Evidence for seed-mediated nucleation in the chemical reduction of gold salts to gold nanoparticles. Chemistry of Materials. 2001;13:2313–2322. doi:10.1021/cm000662n.

[23] Jana NR, Gearheart L, Murphy CJ. Seed-mediated growth approach for shape-controlled synthesis of spheroidal and rod-like gold nanoparticles using a surfactant template. Advanced Materials. 2001;13:1389–1393. doi:10.1002/1521–4095(200109)13:18<1389::aid-adma1389>3.0.co;2-f.

[24] El-Sayed MA. Small is different: shape-, size-, and composition-dependent properties of some colloidal semiconductor nanocrystals. Accounts of Chemical Research. 2004;37:326–333. doi:10.1021/ar020204f.

[25] Semagina N, Kiwi-Minsker L. Recent advances in the liquid-phase synthesis of metal nanostructures with controlled shape and size for catalysis. Catalysis Reviews. 2009;51:147–217. doi:10.1080/01614940802480379.

[26] Pérez-Juste J, Pastoriza-Santos I, Liz-Marzán LM, Mulvaney P. Gold nanorods: synthesis, characterization and applications. Coordination Chemistry Reviews. 2005;249:1870–1901. doi:10.1016/j.ccr.2005.01.030.

[27] Grzelczak M, Perez-Juste J, Mulvaney P, Liz-Marzan LM. Shape control in gold nanoparticle synthesis. Chemical Society Reviews 2008;37:1783–1791. doi:10.1039/B711490G.

[28] Alexandridis P. Gold nanoparticle synthesis, morphology control, and stabilization facilitated by functional polymers. Chemical Engineering & Technology. 2011;34:15–28. doi:10.1002/ceat.201000335.

[29] Nikoobakht B, El-Sayed MA. Preparation and growth mechanism of gold nanorods (NRs) using seed-mediated growth method. Chemistry of Materials. 2003;15:1957–1962. doi:10.1021/cm020732l.

[30] Liu M, Guyot-Sionnest P. Mechanism of silver(I)-assisted growth of gold nanorods and bipyramids. Journal of Physical Chemistry B. 2005;109:22192–22200. doi:10.1021/jp054808n.

[31] Pal T, De, Jana NR, Pradhan N, Mandal R, Pal A, Beezer AE, Mitchell JC. Organized Media as redox catalysts. Langmuir. 1998;14:4724–4730. doi:10.1021/la980057n.

[32] Pérez-Juste J, Liz-Marzán LM, Carnie S, Chan DYC, Mulvaney P. Electric-field-directed growth of gold nanorods in aqueous surfactant solutions. Advanced Functional Materials. 2004;14:571–579. doi:10.1002/adfm.200305068.

[33] Sau TK, Murphy CJ. Seeded high yield synthesis of short au nanorods in aqueous solution. Langmuir. 2004;20:6414–6420. doi:10.1021/la049463z.

[34] Wang ZL. Transmission electron microscopy of shape-controlled nanocrystals and their assemblies. The Journal of Physical Chemistry B. 2000;104:1153–1175. doi:10.1021/jp993593c.

[35] Gao JX, Bender CM, Murphy CJ. Dependence of the gold nanorod aspect ratio on the nature of the directing surfactant in aqueous solution. Langmuir. 2003;19:9065–9070. doi:10.1021/la034919i.

[36] Tollan C, Echeberria J, Marcilla R, Pomposo J, Mecerreyes D. One-step growth of gold nanorods using a β-diketone reducing agent. Journal of Nanoparticle Research. 2009;11:1241–1245. doi:10.1007/s11051-008-9564-z.

[37] Kundu S, Pal A, Ghosh S, Nath S, Panigrahi S, Praharaj S, Basu S, Pal T. Shape-controlled Synthesis of Gold Nanoparticles from Gold(III)-chelates of β-diketones. Journal of Nanoparticle Research. 2005;7:641–650. doi:10.1007/s11051-005-3475-z.

[38] Johnson CJ, Dujardin E, Davis SA, Murphy CJ, Mann S. Growth and form of gold nanorods prepared by seed-mediated, surfactant-directed synthesis. Journal of Materials Chemistry. 2002;12:1765–1770. doi:10.1039/b200953f.

[39] Yang X, Yang M, Pang B, Vara M, Xia Y. Gold nanomaterials at work in biomedicine. Chemical Reviews. 2015;115:10410–10488. doi:10.1021/acs.chemrev.5b00193.

[40] Habrioux A, Servat K, Tingry S, Kokoh KB. Enhancement of the performances of a single concentric glucose/O_2 biofuel cell by combination of bilirubin oxidase/Nafion cathode and Au–Pt anode. Electrochemistry Communications. 2009;11:111–113. doi:10.1016/j.elecom.2008.10.047.

[41] Boutonnet M, Kizling J, Stenius P, Maire G. The preparation of monodisperse colloidal metal particles from microemulsions. Colloids and Surfaces. 1982;5:209–225.

[42] Both Engel A, Bechelany M, Fontaine O, Cherifi A, Cornu D, Tingry S. One-pot route to gold nanoparticles embedded in electrospun carbon fibers as an efficient catalyst material for hybrid alkaline glucose biofuel cells. ChemElectroChem. 2016;3:629–637. doi:10.1002/celc.201500537.

[43] Cheng T-M, Huang T-K, Lin H-K, Tung S-P, Chen Y-L, Lee C-Y, Chiu H-T. (110)-Exposed gold nanocoral electrode as low onset potential selective glucose sensor. ACS Applied Materials & Interfaces. 2010;2:2773–2780. doi:10.1021/am100432a.

[44] Tung S-P, Huang T-K, Lee C-Y, Chiu H-T. Electrochemical growth of gold nanostructures on carbon paper for alkaline direct glucose fuel cell. RSC Advances. 2012;2:1068–1073. doi:10.1039/C1RA00611H.

[45] Herricks T, Chen J, Xia Y. Polyol synthesis of platinum nanoparticles: control of morphology with sodium nitrate. Nano Letters. 2004;4:2367–2371. doi:10.1021/nl048570a.

[46] Holade Y, Servat K, Napporn TW, Kokoh KB. Electrocatalytic properties of nanomaterials synthesized from "Bromide Anion Exchange" method—investigations of glucose and glycerol oxidation. Electrochimica Acta. 2015;162:205–214. doi: http://dx.doi.org/10.1016/j.electacta.2014.11.072.

[47] Holade Y, Morais C, Servat K, Napporn TW, Kokoh KB. Toward the electrochemical valorization of glycerol: Fourier transform infrared spectroscopic and chromatographic studies. ACS Catalysis. 2013;3:2403–2411. doi:10.1021/cs400559d.

[48] Holade Y, Morais C, Arrii-Clacens S, Servat K, Napporn TW, Kokoh KB. New preparation of PdNi/C and PdAg/C nanocatalysts for glycerol electrooxidation in alkaline medium. Electrocatalysis. 2013;4:167–178. doi:10.1007/s12678-013-0138-1.

[49] Lim B, Kobayashi H, Camargo PC, Allard L, Liu J, Xia Y. New insights into the growth mechanism and surface structure of palladium nanocrystals. Nano Research. 2010;3:180–188. doi:10.1007/s12274-010-1021-5.

[50] Holade Y, Sahin N, Servat K, Napporn T, Kokoh K. Recent advances in carbon supported metal nanoparticles preparation for oxygen reduction reaction in low temperature fuel cells. Catalysts. 2015;5:310–348. doi:10.3390/catal5010310.

[51] Holade Y, Servat K, Napporn TW, Morais C, Berjeaud J-M, Kokoh KB. Highly selective oxidation of carbohydrates in an efficient electrochemical energy converter: cogenerating organic electrosynthesis. ChemSusChem. 2016;9:252–263. doi:10.1002/cssc.201501593.

[52] Hamelin A. Cyclic voltammetry at gold single-crystal surfaces. Part 1. Behaviour at low-index faces. Journal of Electroanalytical Chemistry. 1996;407:1–11. doi: http://dx.doi.org/10.1016/0022-0728(95)04499-X.

[53] Juodkazis K, Juodkazyt J, Jasulaitien V, Lukinskas A, Šebeka B. XPS studies on the gold oxide surface layer formation. Electrochemistry Communications. 2000;2:503–507. doi: http://dx.doi.org/10.1016/S1388-2481(00)00069-2.

[54] Burke LD, Nugent PF. The electrochemistry of gold: I the redox behaviour of the metal in aqueous media. Gold Bulletin. 1997;30:43–53. doi:10.1007/bf03214756.

[55] Sánchez-Sánchez CM, Vidal-Iglesias FJ, Solla-Gullón J, Montiel V, Aldaz A, Feliu JM, Herrero E. Scanning electrochemical microscopy for studying electrocatalysis on shape-controlled gold nanoparticles and nanorods. Electrochimica Acta. 2010;55:8252–8257. doi:10.1016/j.electacta.2010.04.010.

[56] Hernandez J, Solla-Gullon J, Herrero E, Feliu JM, Aldaz A. In Situ surface characterization and oxygen reduction reaction on shape-controlled gold nanoparticles. Journal of Nanoscience and Nanotechnology. 2009;9:2256–2273. doi:10.1166/jnn.2009.SE38.

[57] Wang ZL, Mohamed MB, Link S, El-Sayed MA. Crystallographic facets and shapes of gold nanorods of different aspect ratios. Surface Science. 1999;440:L809–L814. doi: 10.1016/S0039-6028(99)00865-1.

[58] Watt GD. A new future for carbohydrate fuel cells. Renewable Energy. 2014;72:99–104. doi: http://dx.doi.org/10.1016/j.renene.2014.06.025.

[59] Ramachandran S, Fontanille P, Pandey A, Larroche C. Gluconic acid: properties, applications and microbial production. Food Technology and Biotechnology. 2006;44:185–195.

[60] Hsiao MW, Adžić RR, Yeager EB. Electrochemical oxidation of glucose on single crystal and polycrystalline gold surfaces in phosphate buffer. Journal of the Electrochemical Society. 1996;143:759–767. doi:10.1149/1.1836536.

[61] Largeaud F, Kokoh KB, Beden B, Lamy C. On the electrochemical reactivity of anomers: electrocatalytic oxidation of α- and β-d-glucose on platinum electrodes in acid and basic media. Journal of Electroanalytical Chemistry. 1995;397:261–269. doi: http://dx.doi.org/10.1016/0022-0728(95)04139-8.

[62] Kokoh KB, Léger JM, Beden B, Lamy C. "On line" chromatographic analysis of the products resulting from the electrocatalytic oxidation of d-glucose on Pt, Au and adatoms modified Pt electrodes-Part I. Acid and neutral media. Electrochimica Acta. 1992;37:1333–1342. doi: http://dx.doi.org/10.1016/0013-4686(92)87004-J.

[63] Hebie S, Holade Y, Maximova K, Sentis M, Delaporte P, Kokoh KB, Napporn TW, Kabashin AV. Advanced electrocatalysts on basis of bare au nanomaterials for biofuel cell applications. ACS Catalysis. 2015;5:6489–6496. doi:10.1021/acscatal.5b01478.

[64] Adzic RR, Hsiao MW, Yeager EB. Electrochemical oxidation of glucose on single crystal gold surfaces. Journal of Electroanalytical Chemistry and Interfacial Electrochemistry. 1989;260:475–485. doi: \doi:10.1016/0022-0728(89)87164-5.

[65] Aoun SB, Dursun Z, Koga T, Bang GS, Sotomura T, Taniguchi I. Effect of metal adlayers on Au(1 1 1) electrodes on electrocatalytic oxidation of glucose in an alkaline solution. Journal of Electroanalytical Chemistry. 2004;567:175–183. doi: http://dx.doi.org/10.1016/j.jelechem.2003.12.022.

[66] Hsiao M-W. The electrochemical oxidation of glucose on single crystal surfaces of gold, PhD thesis at Case Western Reserve University; Order number 9110784, p1–184, 1990, http://rave.ohiolink.edu/etdc/view?acc_num=case1055261843.

[67] Wu B, Zheng N. Surface and interface control of noble metal nanocrystals for catalytic and electrocatalytic applications. Nano Today. 2013;8:168–197. doi: http://dx.doi.org/10.1016/j.nantod.2013.02.006.

[68] Hammer B, Nørskov JK. Theoretical surface science and catalysis-Calculations and concepts. Advances in Catalysis 45:71–129, 2000, doi: 10.1016/S0360–0564(02)45013–4.

[69] Getsoian AB, Zhai Z, Bell AT. Band-gap energy as a descriptor of catalytic activity for propene oxidation over mixed metal oxide catalysts. Journal of the American Chemical Society. 2014;136:13684–13697. doi:10.1021/ja5051555.

[70] Wieckowski A, Savinova ER, Vayenas CG. Catalysis and Electrocatalysis at Nanoparticle Surfaces. New York, NY: Marcel Dekker, Inc.; 2003.

[71] Lahmani M, Bréchignac C, Houdy P. Les Nanosciences: 2. Nanomatériaux Et Nanochimie. 2nd ed. Paris, France: Belin; 2012.

[72] Basu D, Basu S. A study on direct glucose and fructose alkaline fuel cell. Electrochimica Acta. 2010;55:5775–5779. doi:10.1016/j.electacta.2010.05.016.

[73] Basu D, Basu S. Performance studies of Pd–Pt and Pt–Pd–Au catalyst for electrooxidation of glucose in direct glucose fuel cell. International Journal of Hydrogen Energy. 2012;37:4678–4684. doi:10.1016/j.ijhydene.2011.04.158.

[74] Li L, Scott K, Yu EH. A direct glucose alkaline fuel cell using MnO_2–carbon nanocomposite supported gold catalyst for anode glucose oxidation. Journal of Power Sources. 2013;221:1–5. doi:10.1016/j.jpowsour.2012.08.021.

[75] Beden B, Çetin I, Kahyaoglu A, Takky D, Lamy C. Electrocatalytic oxidation of saturated oxygenated compounds on gold electrodes. Journal of Catalysis. 1987;104:37–46. doi: http://dx.doi.org/10.1016/0021-9517(87)90334-4.

[76] Beden B, Largeaud F, Kokoh KB, Lamy C. Fourier transform infrared reflectance spectroscopic investigation of the electrocatalytic oxidation of d-glucose: Identification of reactive intermediates and reaction products. Electrochimica Acta. 1996;41:701–709. doi: http://dx.doi.org/10.1016/0013-4686(95)00359-2.

[77] Kokoh KB, Parpot P, Belgsir EM, Léger JM, Beden B, Lamy C. Selective oxidation of D-gluconic acid on platinum and lead adatoms modified platinum electrodes in alka-

line medium. Electrochimica Acta. 1993;38:1359–1365. doi: http://dx.doi.org/10.1016/0013-4686(93)80070-G.

[78] Yoshida J-i, Kataoka K, Horcajada R, Nagaki A. Modern strategies in electroorganic synthesis. Chemical Reviews. 2008;108:2265–2299. doi:10.1021/cr0680843.

[79] Waldvogel SR, Janza B. Renaissance of electrosynthetic methods for the construction of complex molecules. Angewandte Chemie International Edition. 2014;53:7122–7123. doi:10.1002/anie.201405082.

[80] Frontana-Uribe BA, Little RD, Ibanez JG, Palma A, Vasquez-Medrano R. Organic electrosynthesis: a promising green methodology in organic chemistry. Green Chemistry. 2010;12:2099–2119. doi:10.1039/C0GC00382D.